ATLAS PUB Note
ATL-PHYS-PUB-2019-042
20th October 2019

Methodology for the EFT interpretation of Higgs boson simplified template cross-section results in ATLAS

The ATLAS Collaboration

The Standard Model (SM) Effective Field Theory (EFT) expansion provides a general framework to report deviations between measurements and SM predictions. This framework can be used in the context of the Higgs boson coupling measurements, where ATLAS results are usually reported in terms of simplified template cross-sections (STXS). This note describes techniques developed to interpret the STXS measurements within the framework of the EFT. Parameterizations of the impact on the Higgs sector of BSM phenomena introduced as EFT contributions are developed, both for the Higgs boson production cross sections and decay widths. Techniques are presented to determine the combinations of EFT parameters to which the measurements provide sensitivity, accounting for measurement correlations, and to identify and treat directions in the space of the EFT parameters to which the measurements are not sensitive.

ATL-PHYS-PUB-2019-042
20 October 2019

1 Introduction

An Effective Field Theory (EFT) approach can be used to set model-independent constraints on physics beyond the Standard Model (BSM). This note describes techniques developed for the interpretation of Higgs boson Simplified Template Cross-section (STXS) [1, 2] measurements within the Standard Model EFT (SMEFT) framework [3]. In this work only CP-even dimension-6 operators are considered, using the Warsaw basis [4] which provides a complete set of independent operators allowed by the SM gauge symmetries. These operators affect both the production and the decay of the Higgs boson. The measurements use a modified version of the STXS Stage 1 binning [1] described in Ref. [5].

The note presents a snapshot of ongoing research, primarily meant to allow discussion in the LHC Higgs Cross-Section Working Group General Assembly in October 2019. The methodology should therefore not be considered final, and for this reason no sensitivity figures are presented.

The note is organized as follows: in Section 2, a parametrisation of the STXS production cross-sections and Higgs boson decay rates in terms of SMEFT parameters is presented. This follows a methodology similar to the one followed in Ref. [6] to determine a similar parametrisation in the context of the Higgs Effective Lagrangian model [7]. In Section 3, a technique is described to identify the regions of SMEFT parameter space that can be constrained by the experimental STXS measurements in the $H \to \gamma\gamma$ channel [8] and in a combination of various Higgs boson decay channels [5]. These results are then used to define a subset of SMEFT parameters within which experimental results can be presented.

2 Parametrisation of the impact of BSM phenomena within the SMEFT framework

2.1 Parametrisation of the Higgs boson production cross sections

Within the SMEFT framework, the amplitude for each Higgs boson production and decay process can be described as

$$\mathcal{M}_{\text{SMEFT}} = \left| \mathcal{M}_{\text{SM}} + \sum_i \frac{c_i}{\Lambda^2} \mathcal{M}_i \right|^2 \tag{1}$$

where $\mathcal{M}_{\text{SM}}$ is the SM amplitude, the sum runs over CP-even dimension-6 SMEFT operators O_i, c_i is the Wilson coefficient of the operator O_i, $\mathcal{M}_i$ are amplitudes involving O_i, and $\Lambda = 1\,\text{TeV}$.

The leading-order BSM contributions are therefore proportional to $1/\Lambda^2$ and originate from the interference between the SM amplitude and amplitudes linear in the c_i. Throughout this note, only terms of order $1/\Lambda^2$ are considered, under the assumption that higher order terms can be neglected. The Higgs boson production cross-section in STXS region p can therefore be expressed as:

$$\sigma_p = \sigma_{p,\text{SM}} + \sigma_{p,\text{int}}. \tag{2}$$

The interference contribution $\sigma_{p,\text{int}}$ verifies

$$\frac{\sigma_{p,\text{int}}}{\sigma_{p,\text{SM}}} = 1 + \sum_i A_i^{\sigma_p} c_i \tag{3}$$

Wilson coefficient	Operator
c_{Hbox}	$(H^\dagger H)\Box(H^\dagger H)$
c_{HDD}	$\left(H^\dagger D^\mu H\right)^* \left(H^\dagger D_\mu H\right)$
c_{HG}	$H^\dagger H\, G^A_{\mu\nu} G^{A\mu\nu}$
c_{HB}	$H^\dagger H\, B_{\mu\nu} B^{\mu\nu}$
c_{HW}	$H^\dagger H\, W^I_{\mu\nu} W^{I\mu\nu}$
c_{HWB}	$H^\dagger \tau^I H\, W^I_{\mu\nu} B^{\mu\nu}$
c_{Hl1}	$(H^\dagger i \overleftrightarrow{D}_\mu H)(\bar{l}_p \gamma^\mu l_r)$
c_{Hl3}	$(H^\dagger i \overleftrightarrow{D}^I_\mu H)(\bar{l}_p \tau^I \gamma^\mu l_r)$
c_{He}	$(H^\dagger i \overleftrightarrow{D}_\mu H)(\bar{e}_p \gamma^\mu e_r)$
c_{Hq1}	$(H^\dagger i \overleftrightarrow{D}_\mu H)(\bar{q}_p \gamma^\mu q_r)$
c_{Hq3}	$(H^\dagger i \overleftrightarrow{D}^I_\mu H)(\bar{q}_p \tau^I \gamma^\mu q_r)$
c_{Hu}	$(H^\dagger i \overleftrightarrow{D}_\mu H)(\bar{u}_p \gamma^\mu u_r)$
c_{Hd}	$(H^\dagger i \overleftrightarrow{D}_\mu H)(\bar{d}_p \gamma^\mu d_r)$
$\lvert c_{uG}\rvert$	$(\bar{q}_p \sigma^{\mu\nu} T^A u_r)\widetilde{H}\, G^A_{\mu\nu}$
c_{ll1}	$(\bar{l}_p \gamma_\mu l_r)(\bar{l}_s \gamma^\mu l_t)$

Table 1: Wilson coefficients c_i and corresponding dimension-6 SMEFT operators O_i used in this analysis.

where the $A_i^{\sigma_p}$ are coefficients independent of the c_i which are determined from simulation. Table 1 lists the Wilson coefficients c_i considered in this work, and the corresponding operators.

This computation is performed using the SMEFTsim package [3] within the MadGraph5_aMC@NLO program [9]. Only leading order (LO) computation of QCD and SM electroweak (EW) processes is provided, with additional corrections introducing LO effective couplings to allow the SM Higgs to gluon and Higgs to photon vertices. The cross section parametrisation is therefore expressed as a relative correction to the SM prediction, which is computed at next-to-leading order (NLO) or next-to-next-to-leading order (NNLO) with state-of-the art theory inputs depending on the process, as described in Ref. [5]:

$$\sigma_p(c_i) = \sigma^{\text{(N)NLO}}_{p,\text{SM}} \left(1 + \frac{\sigma^{\text{LO}}_{p,\text{int}}}{\sigma^{\text{LO}}_{p,\text{SM}}}\right) = \sigma^{\text{(N)NLO}}_{p,\text{SM}} \left(1 + \sum_i A_i^{\sigma} c_i\right). \tag{4}$$

This relies on the assumption that the relative corrections to the cross section from the SMEFT are the same at LO and higher orders [10]. Figure 1 shows example comparisons of some of the kinematic distributions relevant for the STXS classification in the $gg \to H$ and EW qqH processes, between a LO computation from MadGraph and the Powheg simulation typically used in published ATLAS Run 2 results.

The dependence of the expected event yield in STXS bin p on the c_i is fully determined by the $A_i^{\sigma_p}$ parameter in Equation 3. These parameters are computed using a set of events samples generated using the SMEFTsim model in MadGraph5_aMC@NLO version 2.6.5 using the process definitions listed in Table 2 for each STXS process. The M_W scheme and $U(3)^5$ flavour structures are used. Interference terms are generated using the `NP^2==1` option. All processes are simulated with the four-flavour scheme (4FS) apart for tHW for which the five-flavour scheme (5FS) is used [9]. The $gg \to ZH$ process is neglected. Events are showered with Pythia version 8.240 [11], using the CKKW-L matching scheme to match matrix element and parton shower computations with different parton multiplicities. Jets are reconstructed from all stable particles with a lifetime greater than 10 ps, excluding the decay products of the Higgs boson and

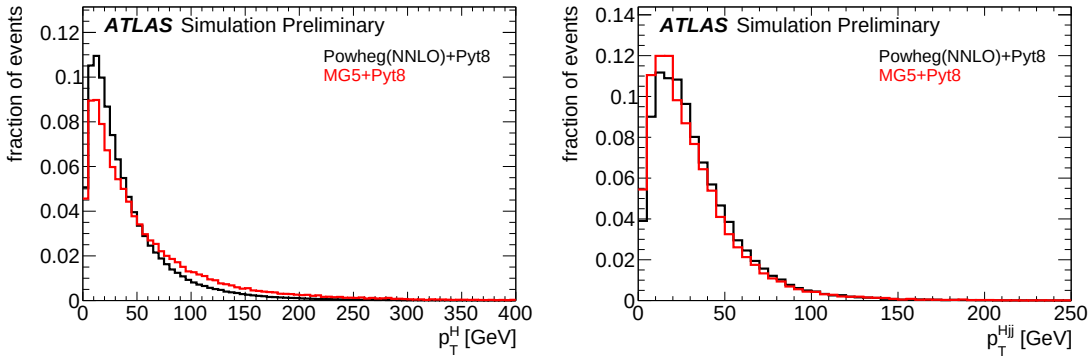

(a) $gg \to H$

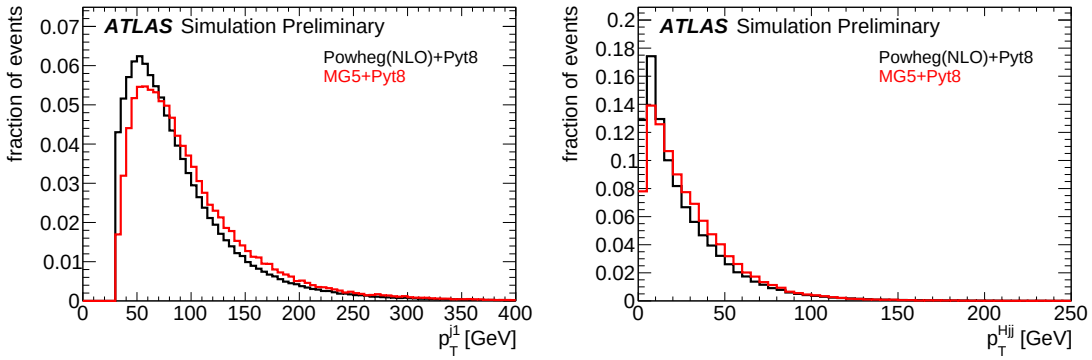

(b) EW qqH

Figure 1: Example comparisons of some of the kinematic distributions used for the STXS classification in the $gg \to H$ (a, b) and EW qqH (c, d) STXS processes. The $gg \to H$ process includes contributions from gluon-gluon fusion (ggF) and $b\bar{b}H$ production, while EW qqH includes vector-boson fusion (VBF) as well as $q\bar{q} \to VH$ production where the vector boson V decays to hadrons. Distributions of events generated assuming the SM parameters with MadGraph5_aMC@NLO (red) and Powheg (black) are shown. MadGraph5_aMC@NLO generation is performed at LO for all processes; Powheg generation is performed at NNLO for the ggF process, and at NLO for the other processes. The Powheg samples are identical to the ones used in the STXS measurements of Refs. [5, 8].

leptons from W and Z boson decays, using the anti-k_t algorithm with a jet radius parameter $R = 0.4$, and must have a transverse momentum $p_{\mathrm{T,jet}} > 30\,\mathrm{GeV}$.

The introduction of new physics impacts the overall cross section, as well as the shape of the kinematic distributions. The variations induced by the most relevant SMEFT operators on the shape of chosen kinematic distributions are shown in Figure 2. These shape variations lead to a different impact in the different measured STXS regions. The shape associated to a non-null c_i coefficient does not depend on the actual c_i value, and is evaluated for $c_i = 1$. The change induced on the total distributions, simultaneously accounting for SM and BSM contributions, would on the other hand depend on their relative importance.

SMEFT modifications to the loop contributions to $gg \to ZH$ are not included in SMEFT, so that only SM contributions are considered for this process. The loop-induced $gg \to H$ and $H \to \gamma\gamma$ processes are treated by SMEFT as effective operators, so that no SMEFT-related modification to these loops are accounted for in this analysis.

SMEFT modifications to the background processes in the included analyses are also not considered.

ggF +bbH	generate p p > h QED=1 add process p p > h j QED=1 add process p p > h j j QED=1 add process p p > h b b~QED=1
VBF +VHhad	generate p p > h j j QCD=0
ZHlep	generate p p > h l+ l-
WHlep	generate p p > h l+ vl add process p p > h l- vl~
ttH	generate p p > h t t~
$tHjb$	generate p p > h t b~j add process p p > h t~b j
tHW (5FS)	define p = p b b~ generate p p > h t w- add process p p > h t~w+

Table 2: Definition of the Higgs boson production modes used for the simulation of events using MadGraph. Here "p" defines the proton in the 4FS, "j" includes the up-, down-, strange- and charm-quark, "l" is a massless lepton (e or μ) and "vl" is a neutrino of any flavour. "~" designates the anti-particle.

Samples are generated for each c_i set to values of -0.5, 0.1 and 1, with the other c_i parameter set at 0 in all cases. The A_i^σ are obtained from a linear fit to the $\sigma_{\text{int}}/\sigma_{\text{SM}}$ value obtained in the 3 cases, considering only the statistical uncertainties on the numbers of generated events.

All SMEFT operators are considered a priori, in order to avoid assumptions on the value of specific Wilson coefficients and therefore to ensure that the result can be used as part of wider fits including constraints from other measurements. However the effect of a coefficient c_i is discarded from the parametrisation of a given STXS cross-section if a relative variation of less than 0.1% is found between the cross-section computed in the SM case and with $c_i = 1$. The 0.1% threshold is chosen in order to ensure that the neglected contributions are negligible compared to the experimental sensitivity, for the range of values considered for each Wilson coefficient ($-10 < c_i < 10$). The conditions also ensure that the computed impacts are larger than the uncertainties due to limited numbers of simulated events. The resulting parametrisation is shown in Table 3. Note that, as stated before, this parametrisation is valid for $\Lambda = 1$ TeV: if one wanted to recast the parametrisation for a different Λ value, the coefficients in Table 3 would need to be rescaled by $(1\,\text{TeV}/\Lambda)^2$.

A representation of the largest variations is shown in Figure 3. More parameters become relevant when considering also Higgs boson decay processes, as described in Section 2.2.

2.2 Parametrisation of the Higgs boson decay widths

The dependence of the Higgs boson partial decay width Γ_f for the $H \to f$ process on the Wilson coefficients can be expressed as

$$\Gamma^f(c_i) = \Gamma^f_{\text{SM}} + \Gamma^f_{\text{int}} = \Gamma^{f,\text{SM}} \left(1 + \sum_i A_i^{\Gamma_f} c_i\right). \tag{5}$$

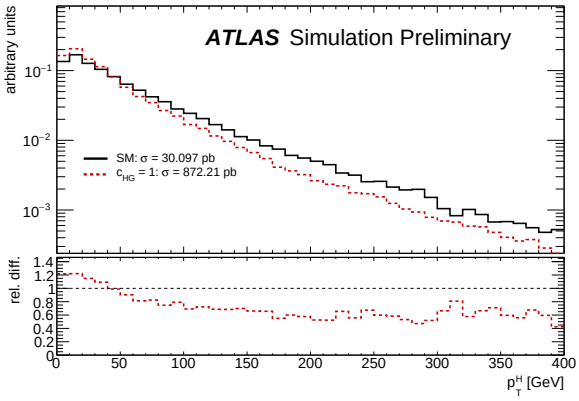

(a) $gg \to H$

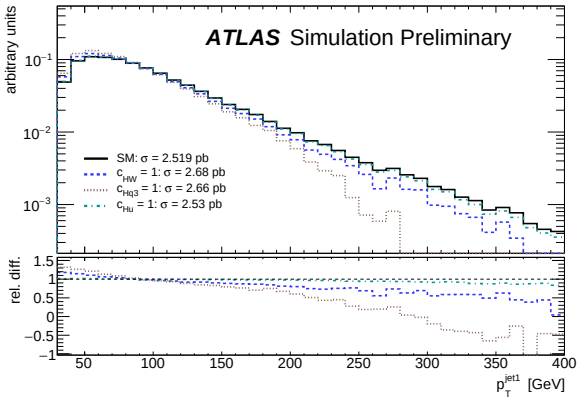

(b) EW qqH

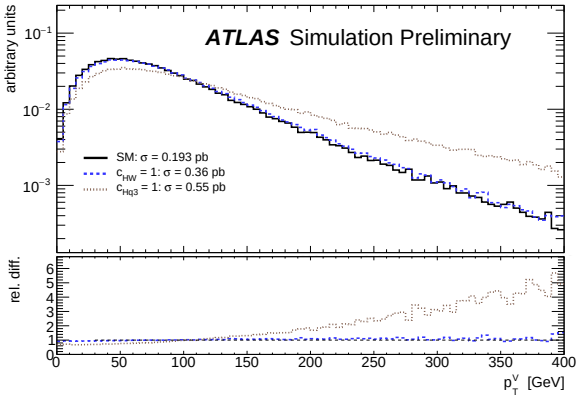

(c) leptonic WH

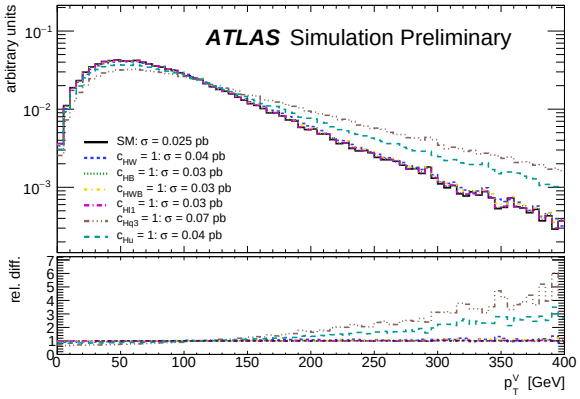

(d) leptonic ZH

Figure 2: Kinematic distributions used for the STXS classification in different production modes, impacted by the interference term for the most relevant SMEFT operators. The STXS processes shown are $gg \to H$ (a), EW qqH (b) and WH (c) and ZH (d) production with leptonic decays of the weak vector boson. The distributions are normalised to unity in order to show the shape differences. The bottom insets show the ratios of the modified distributions to the SM.

Measured region	$\sigma_{\text{int}}/\sigma_{\text{SM}}$
$gg \to H$ (0-jet)	$35.0 \cdot c_{HG}$
$gg \to H$ (1-jet, $p_{\text{T}}^{H} < 60\,\text{GeV}$)	$28.3 \cdot c_{HG}$
$gg \to H$ (1-jet, $60 < p_{\text{T}}^{H} < 120\,\text{GeV}$)	$26.1 \cdot c_{HG}$
$gg \to H$ (1-jet, $120 < p_{\text{T}}^{H} < 200\,\text{GeV}$)	$23.1 \cdot c_{HG}$
$gg \to H$ ($\geq$ 2-jet, $p_{\text{T}}^{H} < 200\,\text{GeV}$)	$16.0 \cdot c_{HG}$
$gg \to H$ ($\geq$ 1-jet, $p_{\text{T}}^{H} > 200\,\text{GeV}$)	$15.6 \cdot c_{HG}$
$qq \to Hqq$ (non-VH)	$0.1213 \cdot c_{Hbox} - 0.0107 \cdot c_{HDD} - 0.008 \cdot c_{HW} + 0.0313 \cdot c_{HWB} - 0.364 \cdot c_{Hl3} + 0.0043 \cdot c_{Hq1} - 0.212 \cdot c_{Hq3} - 0.0108 \cdot c_{Hu} + 0.0038 \cdot c_{Hd} + 0.182 \cdot c_{ll1}$
$qq \to Hqq$ (VH)	$0.120 \cdot c_{Hbox} - 0.0071 \cdot c_{HDD} + 0.623 \cdot c_{HW} + 0.0215 \cdot c_{HB} + 0.098 \cdot c_{HWB} - 0.360 \cdot c_{Hl3} - 0.026 \cdot c_{Hq1} + 1.86 \cdot c_{Hq3} + 0.135 \cdot c_{Hu} - 0.0506 \cdot c_{Hd} + 0.181 \cdot c_{ll1}$
$qq \to Hqq$ ($p_{\text{T,jet1}} > 200\,\text{GeV}$)	$0.122 \cdot c_{Hbox} - 0.0073 \cdot c_{HDD} - 0.25 \cdot c_{HW} + 0.0024 \cdot c_{HB} + 0.045 \cdot c_{HWB} - 0.367 \cdot c_{Hl3} + 0.030 \cdot c_{Hq1} - 0.47 \cdot c_{Hq3} - 0.030 \cdot c_{Hu} + 0.0087 \cdot c_{Hd} + 0.180 \cdot c_{ll1}$
$qq \to H\ell\nu$ ($p_{\text{T}}^{V} < 250\,\text{GeV}$)	$0.1212 \cdot c_{Hbox} - 0.0304 \cdot c_{HDD} + 0.874 \cdot c_{HW} - 0.242 \cdot c_{Hl3} + 1.710 \cdot c_{Hq3} + 0.182 \cdot c_{ll1}$
$qq \to H\ell\nu$ ($p_{\text{T}}^{V} > 250\,\text{GeV}$)	$0.121 \cdot c_{Hbox} - 0.0299 \cdot c_{HDD} + 1.06 \cdot c_{HW} - 0.237 \cdot c_{Hl3} + 10.9 \cdot c_{Hq3} + 0.184 \cdot c_{ll1}$
$qq/gg \to H\ell\ell$ ($p_{\text{T}}^{V} < 150\,\text{GeV}$)	$0.1218 \cdot c_{Hbox} + 0.0259 \cdot c_{HDD} + 0.696 \cdot c_{HW} + 0.0846 \cdot c_{HB} + 0.328 \cdot c_{HWB} + 0.1332 \cdot c_{Hl1} - 0.231 \cdot c_{Hl3} - 0.1076 \cdot c_{He} + 0.016 \cdot c_{Hq1} + 1.409 \cdot c_{Hq3} + 0.315 \cdot c_{Hu} - 0.1294 \cdot c_{Hd} + 0.182 \cdot c_{ll1}$
$qq/gg \to H\ell\ell$ ($150 < p_{\text{T}}^{V} < 250\,\text{GeV}$)	$0.124 \cdot c_{Hbox} + 0.026 \cdot c_{HDD} + 0.85 \cdot c_{HW} + 0.102 \cdot c_{HB} + 0.389 \cdot c_{HWB} + 0.134 \cdot c_{Hl1} - 0.232 \cdot c_{Hl3} - 0.109 \cdot c_{He} - 0.16 \cdot c_{Hq1} + 3.56 \cdot c_{Hq3} + 0.85 \cdot c_{Hu} - 0.315 \cdot c_{Hd} + 0.184 \cdot c_{ll1}$
$qq/gg \to H\ell\ell$ ($p_{\text{T}}^{V} > 250\,\text{GeV}$)	$0.122 \cdot c_{Hbox} + 0.028 \cdot c_{HDD} + 0.88 \cdot c_{HW} + 0.121 \cdot c_{HB} + 0.43 \cdot c_{HWB} + 0.137 \cdot c_{Hl1} - 0.234 \cdot c_{Hl3} - 0.113 \cdot c_{He} - 0.82 \cdot c_{Hq1} + 8.5 \cdot c_{Hq3} + 2.14 \cdot c_{Hu} - 0.71 \cdot c_{Hd} + 0.182 \cdot c_{ll1}$
$ttH + tH$	$0.133 \cdot c_{G} + 0.1182 \cdot c_{Hbox} - 0.0296 \cdot c_{HDD} + 0.532 \cdot c_{HG} + 0.0120 \cdot c_{HW} - 0.1152 \cdot \lvert c_{uH} \rvert - 0.790 \cdot \lvert c_{uG} \rvert - 0.0111 \cdot \lvert c_{uW} \rvert - 0.0017 \cdot \lvert c_{uB} \rvert - 0.1320 \cdot c_{Hl3} + 0.0146 \cdot c_{Hq3} + 0.0660 \cdot c_{ll1} + 0.0218 \cdot c_{qq1} + 0.1601 c_{qq11} + 0.0263 \cdot c_{qq3} + 0.388 c_{qq31} + 0.0114 \cdot c_{uu} + 0.1681 \cdot c_{uu1} - 0.0018 \cdot c_{ud1} + 0.0265 \cdot c_{ud8} + 0.007 \cdot c_{qu1} + 0.1087 \cdot c_{qu8} - 0.0011 \cdot c_{qd1} + 0.0266 \cdot c_{qd8}$

Table 3: Parametrisation of the cross section in the measured STXS regions considering the interference terms. The linear coefficients of the dependence of each cross-section value on the Wilson coefficients are shown. Only terms with factors greater than 0.1% in front of the Wilson coefficient are considered. While expected to be non-negligible in some of the decay channels (e.g. $H \to 4\ell$), the acceptance dependence on the Wilson coefficients is neglected in this parametrisation. The parametrisation is valid for $\Lambda = 1\,\text{TeV}$.

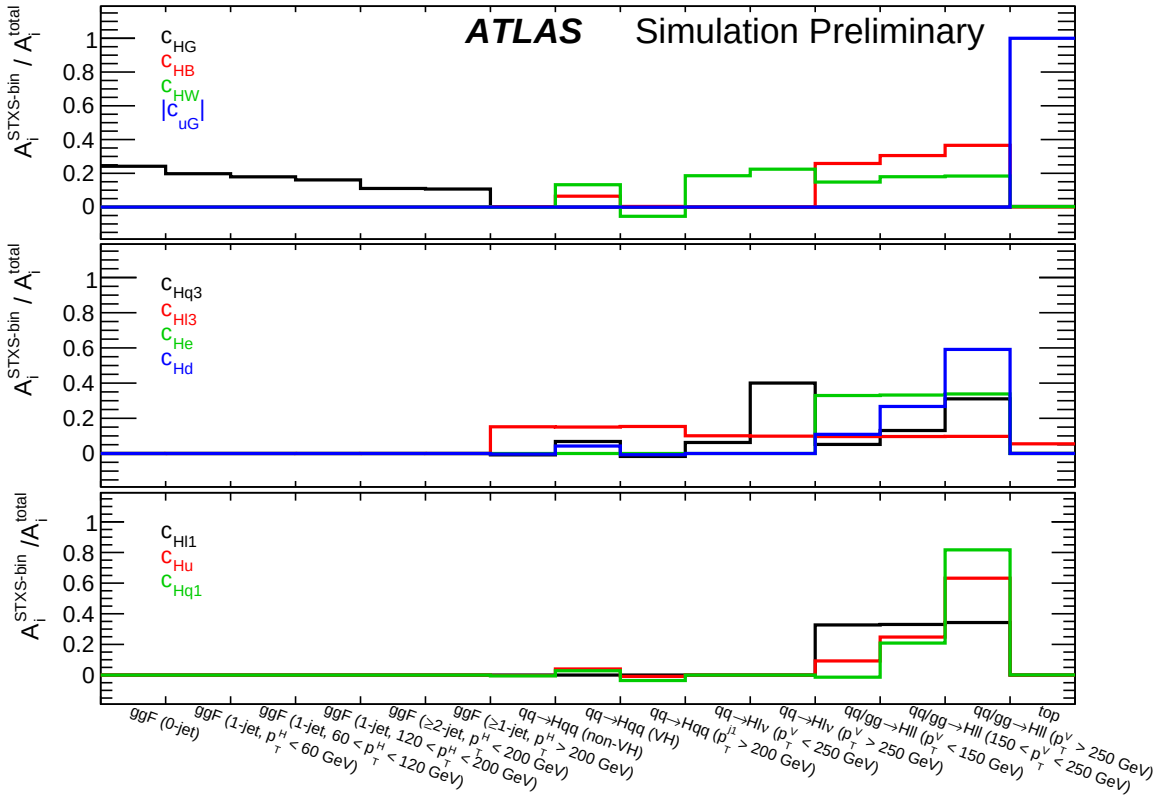

Figure 3: Relative impact of selected SMEFT operators on the cross-section in each STXS bin, defined as the $A_i^{\sigma_p}$ factor for the given STXS bin and Wilson coefficient c_i divided by the sum $\sum_p A_i^{\sigma_p}$ over all STXS bins. The operators with the largest expected sensitivity in the parametrisation of the production mode cross sections are shown. Each histogram is normalised to one to visualise better the relative change in each STXS bin.

where $\Gamma^{f,\text{SM}}$ is the SM value of the decay width, obtained as described in Ref. [5], and $A_i^{\Gamma f}$ are parameters obtained from simulation. The relation is derived using the same assumptions as in Section 2.1, in particular neglecting terms beyond $1/\Lambda^2$.

The parameters $A_i^{\Gamma f}$ are obtained by generating each of the measured Higgs boson decay processes using SMEFTsim, using the same procedure as described in Section 2.1 and the generator configurations listed in Table 4. The parametrisations are derived by considering the full phase space of each decay, with the Higgs boson decaying at rest. Samples corresponding to $c_i = 1$ are generated for each Wilson coefficient in turn, with the other coefficients set to 0. The $A_i^{\Gamma f}$ are determined from the relative variations in event rates between these samples and the SM.

The dependence of the experimental acceptance on the Wilson coefficients is not considered in this study. This dependence is expected to be sizable in particular for decays to weak vector bosons (e.g. $H \to 4\ell$). This could have an effect on the sensitivities reported in this note, but the methodology used should remain applicable in the same way in future work where this dependence is accounted for.

The final parametrisations of the decay widths for all decay channels included in the combination, as well as of the total Higgs boson width, are listed in Table 5.

$H \to 4\ell$	generate h > l+ l- l+ l-
$H \to \ell\nu\ell\nu$	generate h > l+ vl l+ vl~
$H \to b\bar{b}$	generate h > b b~
$H \to \tau^+\tau^-$	generate h > ta+ ta-
$H \to \gamma\gamma$	generate h > a a
Additional channels entering total width	
$H \to \tau^+\nu_\tau\tau^-\bar{\nu}_\tau$	generate h > ta+ vt ta- vt
$H \to \ell\nu_\ell\tau\nu_\tau$	generate h > l+ vl ta- vt add process h > ta+ vt l- vl
$H \to jj\ell(\tau)\nu$	generate h > l+ vl j j add process h > j j l- vl add process h > ta+ vt j j add process h > j j ta- vt
$H \to 4j$	generate h > j j j j
$H \to 4\tau$	generate h > ta+ ta- ta+ ta-
$H \to 4\nu$	generate h > vl vl vl vl add process h > vt vt vt vt add process h > vt vt vl vl
$H \to \ell^+\ell^-\tau^+\tau^-$	generate h > l+ l- ta+ ta-
$H \to 2\nu 2\ell(\tau)$	generate h > vl vl ta+ ta- add process h > vt vt l+ l-
$H \to 2j2\ell(\tau)$	generate h > j j l+ l- add process h > j j ta+ ta-
$H \to 2j2\nu$	generate h > j j vl vl add process h > j j vt vt
$H \to c\bar{c}$	generate h > c c
$H \to s\bar{s}$	generate h > s s
$H \to \mu^+\mu^-$	generate h > mu+ mu-
$H \to e^+e^-$	generate h > e+ e-
$H \to Z\gamma$	generate h > z a
$H \to gg$	generate h > g g

Table 4: Definition of the Higgs boson decay modes used for the simulation of events using MadGraph. For the two-body decays into light fermions, the massive scheme is used to obtain a non-zero decay width.

Channel	$\Gamma_{\text{int}}/\Gamma_{\text{SM}}$
$H \to \gamma\gamma$	$-13.996 \cdot c_{HW} - 48.809 \cdot c_{HB} + 26.144 \cdot c_{HWB}$
$H \to 4\ell$	$0.119 \cdot c_{Hbox} + 0.005 \cdot c_{HDD} - 0.296 \cdot c_{HW} - 0.197 \cdot c_{HB} + 0.296 \cdot c_{HWB} + 0.126 \cdot c_{Hl1} - 0.234 \cdot c_{Hl3} - 0.101 \cdot c_{He} + 0.181 \cdot c_{ll1}$
$H \to \ell\nu\ell\nu$	$0.121 \cdot c_{Hbox} - 0.031 \cdot c_{HDD} - 0.095 \cdot c_{HW} + 0.006 \cdot c_{HB} + 0.002 \cdot c_{HWB} - 0.228 \cdot c_{Hl3} - 0.004 \cdot c_{He} + 0.181 \cdot c_{ll1}$
$H \to \tau\tau$	$0.121 \cdot c_{Hbox} - 0.030 \cdot c_{HDD} - 0.121 \cdot \lvert c_{eH}\rvert - 0.121 \cdot c_{Hl3} + 0.061 \cdot c_{ll1}$
$H \to b\bar{b}$	$0.121 \cdot c_{Hbox} - 0.030 \cdot c_{HDD} - 0.121 \cdot \lvert c_{dH}\rvert - 0.121 \cdot c_{Hl3} + 0.061 \cdot c_{ll1}$
Total	$0.117 \cdot c_{Hbox} - 0.029 \cdot c_{HDD} + 1.362 \cdot c_{HG} - 0.050 \cdot c_{HW} - 0.063 \cdot c_{HB} + 0.052 \cdot c_{HWB} - 0.005 \cdot \lvert c_{eH}\rvert - 0.008 \cdot \lvert c_{uH}\rvert - 0.085 \cdot \lvert c_{dH}\rvert - 0.146 \cdot c_{Hl3} + 0.013 \cdot c_{Hq3} + 0.076 \cdot c_{ll1}$

Table 5: Parametrisation of the decay widths of the considered Higgs boson decays as well as for the total Higgs boson width. Only terms with factors greater than 0.1% in front of the Wilson coefficient are considered. While expected to be non-negligible in some of the decay channels (e.g. $H \to 4\ell$), the acceptance dependence on the Wilson coefficients is neglected in this parametrisation. This parametrisation is valid for $\Lambda = 1$ TeV.

2.3 Parametrisation of the event yields

Assuming the Higgs boson to be a narrow-width, scalar particle as in the SM, its production cross sections factorise from its partial decay widths. The parametrisation of the cross-section in a given STXS bin p and a given decay mode $H \to f$ can thus be derived from those of the production and decay processes separately as

$$\sigma_p \cdot \mathcal{B}^{H\to f} = \left(\sigma_{p,\text{SM}} + \sigma_{p,\text{int}}\right) \cdot \frac{\Gamma^f_{\text{SM}} + \Gamma^f_{\text{int}}}{\Gamma_{\text{SM}} + \Gamma_{\text{int}}}, \tag{6}$$

neglecting as before terms beyond $1/\Lambda^2$. The terms Γ_{SM} and $\Gamma_{\text{int}} = \Gamma_{\text{SM}} \sum_i A^\Gamma_i c_i$ denote respectively the SM and interference contributions to the total Higgs boson width. They are computed as the sum of the corresponding terms for all partial widths, computed in Section 2.2, considering up to four-body decays. At first order in $\Gamma_{\text{int}}/\Gamma_{\text{SM}}$, and neglecting terms of order $1/\Lambda^4$ and higher, one has

$$\sigma_p \cdot \mathcal{B}^{H\to f} = \left[\sigma_p \cdot \mathcal{B}^{H\to f}\right]_{\text{SM}} \left(1 + \frac{\sigma_{\text{p,int}}}{\sigma_{p,\text{SM}}} + \frac{\mathcal{B}^{H\to f}_{\text{int}}}{\mathcal{B}^{H\to f}_{\text{SM}}}\right) \tag{7}$$

$$= \left[\sigma_p \cdot \mathcal{B}^{H\to f}\right]_{\text{SM}} \left(1 + \sum_i A_i^{\sigma_p} c_i + \sum_i \left(A_i^{\Gamma_f} - A_i^{\Gamma}\right) c_i\right) \tag{8}$$

$$= \left[\sigma_p \cdot \mathcal{B}^{H\to f}\right]_{\text{SM}} \left(1 + \sum_i A_i^{\sigma_p \cdot \mathcal{B}^{H\to f}} c_i\right). \tag{9}$$

where $\mathcal{B}^{H\to f}_{\text{SM}}$ and $\mathcal{B}^{H\to f}_{\text{int}}$ are respectively the SM and interference contributions to the $H \to f$ branching ratio.

3 Constraints on the Wilson Coefficients from STXS measurements

Constraints on Wilson coefficients can be obtained from the STXS measurements in the $H \to \gamma\gamma$ channel of Ref. [8] and in the combination of decay channels of Ref. [5]. These measurements are based on likelihoods in which the expected yield in each STXS bin includes a signal strength modifier, which can be reparametrised using Equation 9, to account for SMEFT modifications to both production and decay; or Equation 4, to account for SMEFT modifications to production only. A fit is then performed to constrain the SMEFT parameters.

In the following, the $H \to \gamma\gamma$ measurement is considered alone since it already provides a good sensitivity to some SMEFT parameters, and as a benchmark for the methodology itself. Since neither the $H \to \gamma\gamma$ nor the combined measurement allow to constrain all Wilson coefficients, only a subset of the parameters must be included in the analysis.

The following sections present a method to define an appropriate subset of parameters, and its application to the analyses listed above. Since this note only aims to discuss these methodological aspects, the full results of the fits are not presented.

3.1 Choice of fitted Wilson coefficients

Combinations of Wilson coefficients to which measurements are not sensitive manifest themselves as *flat* directions in the likelihood, along which the likelihood exhibits no curvature as one moves away from regions where the likelihood is maximal. These directions can in principle be identified using the Fisher information matrix of the likelihood at its maximum, defined as the inverse of the covariance matrix produced by minimization algorithms such as Minuit.

However the minimization is generally unstable due to the presence of the flat directions, so an alternate procedure is followed. One starts from the Fisher information matrix C^{-1}_{STXS} of the original measurement likelihood, parametrised in terms of the STXS parameters. Since this likelihood is free of flat directions, C_{STXS} can be obtained using the HESSE method within Minuit [12]. The Fisher information matrix of the SMEFT measurement is then obtained by propagating the parametrisation of the STXS cross sections through C^{-1}_{STXS}. For the case of a parametrisation involving only the production cross-section, one has

$$C^{-1}_{\text{EFT}} = P^T \, C^{-1}_{\text{STXS}} \, P, \tag{10}$$

with the parametrisation matrix

$$P = \begin{pmatrix} A_1^{\sigma_1} & A_2^{\sigma_1} & A_3^{\sigma_1} & \dots \\ A_1^{\sigma_2} & A_2^{\sigma_2} & A_3^{\sigma_2} & \dots \\ A_1^{\sigma_3} & A_2^{\sigma_3} & A_3^{\sigma_3} & \dots \\ \vdots & \vdots & \vdots & \end{pmatrix}, \tag{11}$$

where the $A_i^{\sigma_p}$ are the linear parameters from Equation 3. The rows of P run over STXS regions, as do the dimensions of C^{-1}_{STXS}. For the case of parameterizing both production and decay, the elements of P are the $A_i^{\sigma_p \cdot \mathcal{B}^{H\to f}}$ and its rows run over the production and decay combinations $\sigma_p \cdot \mathcal{B}^{H\to f}$, as do the dimensions of C^{-1}_{STXS}.

In the approximation of a Gaussian likelihood for the STXS measurement, C^{-1}_{EFT} is the exact Fisher information matrix of its SMEFT re-parametrisation. The sensitivity of the measurement to combinations

of Wilson coefficients is mapped out by the eigenvalues and eigenvectors of C^{-1}_{STXS}. In the Gaussian approximation, each eigenvector with eigenvalue F_α corresponds to an independent measurement with an uncertainty $\sigma_\alpha = 1/\sqrt{F_\alpha}$. Large eigenvalues thus correspond to eigenvectors with high experimental sensitivity, while null eigenvalues identify flat directions.

Since the procedure relies on a Gaussian approximation, it only serves as a guideline to identify the parameter combination in which the measurement results can be reported. The results themselves can then be obtained in the usual way from a likelihood fit after re-parameterizing into the new measurement basis. The latter can be determined from the eigenvalue decomposition of C^{-1}_{EFT} in the following ways:

- A combination of parameters associated with flat directions can be excluded from the analysis, for instance by fixing its value to 0 in the likelihood fit. In general this procedure introduces a model assumption, and therefore reduces the reinterpretability of the results and does not allow for an easy combination with new measurements possibly sensitive to the combination that was set to zero. However in the case of a flat direction this has no impact on the result, since the likelihood does not depend on the fixed parameter, and the procedure is therefore safe. The same applies to cases where the eigenvalues are non-zero but correspond to uncertainties that are much larger than those of other measurements, for instance from precision electroweak data. If the other measurements are assumed to always be included in the analysis, then quasi-flat directions with sufficiently small eigenvalues do not contribute to the final measurement and can also be safely fixed to 0.
- In some cases, different operators have a similar impact on all STXS regions, and therefore cannot be disentangled by the measurement. In this case only some combinations of the parameters are constrained by the measurement, and it makes sense to use these combinations as the new measurement parameters. The orthogonal directions are flat directions, which can be fixed to 0 as described above.

The final choice of Wilson coefficients can be validated by testing the convergence properties of the likelihood fit in this parametrisation.

The procedure is performed on the likelihood of the expected STXS measurements, in order to avoid biases from features in the data. In practice, the Fisher information matrix is obtained from a fit to an Asimov dataset [13] generated in the SM hypothesis, with nuisance parameters set to their best-fit values in a fit to the data conditional on the SM hypothesis.

In this note, only the eigenvectors with eigenvalue larger than ~0.1 are taken into account. This ensures that the eigenvectors that are not considered correspond to quasi-flat directions, for the range of Wilson coefficient values considered in this note ($-10 < c_i < 10$).

To understand the physical origin of the measurement sensitivity to the SMEFT operators, this procedure is applied to different scenarios corresponding to parameterizing the production cross-sections only, or both the production cross-section and decay branching ratios, and using the $H \to \gamma\gamma$ decay only or the combination of measurements in several decay channels. As noted in Section 2.2, the dependence of the experimental acceptance on the Wilson coefficients is not considered in the parametrisation of decay branching ratios.

Eigenvalue	Eigenvector
95892.10	$-1.00 \cdot c_{HG}$
620	$-0.24 \cdot c_{HW} + 0.13 \cdot c_{Hl3} - 0.95 \cdot c_{Hq3}$
34	$-0.14 \cdot c_G - 0.13 \cdot c_{Hbox} + 0.16 \cdot c_{Hl3} + 0.12 \cdot \lvert c_{uH}\rvert + 0.82 \cdot \lvert c_{uG}\rvert - 0.17 \cdot cqq_{11} - 0.40 \cdot cqq_{31} - 0.18 \cdot c_{uu1} - 0.11 \cdot c_{qu8}$
10	$-0.64 \cdot c_{HW} + 0.18 \cdot c_{HWB} + 0.23 \cdot c_{Hl3} - 0.18 \cdot c_{Hq1} + 0.14 \cdot c_{Hq3} + 0.60 \cdot c_{Hu} - 0.21 \cdot c_{Hd} - 0.14 \cdot c_{ll1}$
7	$0.56 \cdot c_{HW} + 0.35 \cdot c_{HWB} + 0.12 \cdot c_{Hl1} - 0.23 \cdot c_{Hl3} - 0.26 \cdot c_{Hq3} + 0.57 \cdot c_{Hu} - 0.21 \cdot c_{Hd} + 0.15 \cdot c_{ll1}$
3	$0.22 \cdot c_{Hbox} - 0.43 \cdot c_{HW} - 0.77 \cdot c_{Hl3} + 0.35 \cdot c_{ll1} + 0.15 \cdot \lvert c_{uG}\rvert$
0.4	$-0.12 \cdot c_{HDD} + 0.69 \cdot c_{HW} - 0.14 \cdot c_{HB} - 0.57 \cdot c_{HWB} - 0.27 \cdot c_{Hl1} - 0.28 \cdot c_{Hl3} + 0.22 \cdot c_{He} - 0.57 \cdot c_{Hq1} + 1.99 \cdot c_{Hq3} + 0.44 \cdot c_{Hu} + 0.12 \cdot c_{ll1}$

Table 6: Eigenvectors corresponding to the largest eigenvalues of the Fisher information matrix of the $H \to \gamma\gamma$ measurement of Ref. [8], expressed as a function of Wilson coefficients. The Fisher information matrix is obtained by propagating the parametrisation of the STXS cross sections through C^{-1}_{STXS}, fixing the branching ratios to their SM values. Only Wilson coefficients with a factor larger than 10% are listed for each eigenvector.

3.1.1 Combined measurement with production cross-section parametrisation only

The combined STXS measurement of Ref. [8] is considered, with the values of the branching ratios fixed to their SM prediction and only the STXS cross sections parametrised as a function of the Wilson coefficients. The eigenvectors obtained from the procedure described in the previous section are shown in Table 6.

The parameters that are expected to be most precisely constrained by the $H \to \gamma\gamma$ STXS measurements are $c_{HG}, c_{Hq3}, |c_{uG}|, c_{HW}, c_{Hu}$, c_{Hl3}, and potentially c_{Hq1}, as determined from the magnitude of the eigenvalues where they appear and of their coefficient in the eigenvector. Parameterizing also the branching ratios in terms of SMEFT operators adds sensitivity to further parameters, but also introduces further correlations between them.

3.1.2 Measurement in the $H \to \gamma\gamma$ channel with production and decay parametrisation

The STXS measurement in the $H \to \gamma\gamma$ channel [8] is considered, now with both production cross-sections and the $H \to \gamma\gamma$ branching ratio parametrised as a function of the Wilson coefficients. The computed eigenvectors are shown in Table 7.

The $H \to \gamma\gamma$ decay parametrisation introduces additional sensitivity to c_{HB} and c_{HWB}, compared to the production rate measurement only. However, due to the excellent sensitivity of the $H \to \gamma\gamma$ measurement to the $gg \to H$ production mode, the measurement of these parameters is mainly driven by the measurement in the analysis region targeting $gg \to H$ production. They are thus strongly correlated with the measurement of c_{HG}. In general, the introduction of the decay parametrisation from a single channel introduces strong correlations with respect to the measurement of the production side only.

Eigenvalue	Eigenvector
504594	$0.16 \cdot c_{HG} - 0.24 \cdot c_{HW} - 0.84 \cdot c_{HB} + 0.45 \cdot c_{HWB}$
14290	$-0.99 \cdot c_{HG} - 0.14 \cdot c_{HB}$
63	$0.14 \cdot c_{HW} + 0.96 \cdot c_{Hq3} + 0.11 \cdot c_{Hu} + 0.15 \cdot \lvert c_{uG} \rvert$
7	$-0.11 \cdot c_G + 0.50 \cdot c_{HW} - 0.13 \cdot c_{HB} - 0.11 \cdot c_{Hl3} + 0.11 \cdot c_{Hq1} - 0.18 \cdot c_{Hq3} - 0.26 \cdot c_{Hu} + 0.65 \cdot \lvert c_{uG} \rvert - 0.13 c_{qq11} - 0.32 c_{qq31} - 0.14 \cdot c_{uu1}$
3	$0.56 \cdot c_{HW} - 0.18 \cdot c_{HB} + 0.15 \cdot c_{Hl3} + 0.18 \cdot c_{Hq1} - 0.49 \cdot c_{Hu} + 0.16 \cdot c_{Hd} - 0.47 \cdot \lvert c_{uG} \rvert + 0.23 c_{qq31}$
2	$-0.59 \cdot c_{HW} - 0.25 \cdot c_{HWB} + 0.20 \cdot c_{Hq1} + 0.16 \cdot c_{Hq3} - 0.65 \cdot c_{Hu} + 0.23 \cdot c_{Hd} + 0.12 \cdot \lvert c_{uG} \rvert$
0.2	$-0.20 \cdot c_{Hbox} - 0.21 \cdot c_{HB} - 0.40 \cdot c_{HWB} + 0.75 \cdot c_{Hl3} - 0.24 \cdot c_{Hq1} - 0.27 \cdot c_{ll1} + 0.16 \cdot \lvert c_{uG} \rvert$
0.1	$0.11 \cdot c_{Hbox} - 0.12 \cdot c_{HDD} - 0.30 \cdot c_{HB} - 0.53 \cdot c_{HWB} - 0.31 \cdot c_{Hl1} - 0.47 \cdot c_{Hl3} + 0.25 \cdot c_{He} - 0.41 \cdot c_{Hq1} + 0.11 \cdot c_{Hu} + 0.16 \cdot c_{ll1}$

Table 7: Eigenvectors corresponding to the largest eigenvalues of the Fisher information matrix of the $H \to \gamma\gamma$ measurement of Ref. [8], expressed as a function of Wilson coefficients. The Fisher information matrix is obtained by propagating the parametrisation of the STXS cross sections through C^{-1}_{STXS}, fixing the branching ratios to their SM values. Both the production cross-sections and the decay branching ratios are parametrised as a function of the Wilson coefficients. Only Wilson coefficients with a factor larger than 10% are listed for each eigenvector. The acceptance dependence on the Wilson coefficients is neglected in the parametrisation.

3.1.3 Combined measurement with production and decay parametrisation

Finally, the combined measurement of Ref. [5] is considered again, but all products of STXS regions and decay processes are included in the parameterization, with the exception of the $H \to b\bar{b}$ decays in the $gg \to H$ and EW qqH regions which are poorly measured. The resulting set of $\sigma_p \cdot \mathcal{B}^{H\to f}$ parameters are expressed in terms of Wilson coefficients using the expression in Equation 9. The eigenvectors for this case are shown in Table 8.

The combination with the measurement in multiple Higgs boson decay channels allows a more precise determination of the Wilson coefficients, and reduces the correlation between the parameters constrained mainly by the production cross sections with those constrained mainly from the Higgs boson decay.

In addition, more operators can be constrained. In particular, this concerns c_{Hl1}, c_{He} and c_{Hd} due to the precise measurement of VH production with leptonic decays of the weak vector boson in the $H \to b\bar{b}$ channel. The $|c_{eH}|$ and $|c_{dH}|$ parameters are also constrained by the $H \to \tau\tau$ and $H \to b\bar{b}$ decays respectively.

From this study, the full list of operators that can be constrained in the combined STXS measurement is: $c_{HG}, c_{Hq3}, c_{HW}, c_{HB}, c_{HWB}, |c_{uG}|, c_{Hl3}, c_{Hl1}, c_{He}, |c_{eH}|, |c_{dH}|, c_{Hd}, c_{Hu}$ and c_{Hq1}. However, the correlations between them can reduce further the number of sensitive "directions".

3.2 Treatment of correlations and flat directions

In this section, the set of parameters obtained in Section 3.1.3 is studied further in order to identify more precisely the directions with strong and weak experimental sensitivity.

Eigenvalue	Eigenvector
241550	$0.24 \cdot c_{HG} - 0.23 \cdot c_{HW} - 0.83 \cdot c_{HB} + 0.45 \cdot c_{HWB}$
147981	$-0.97 \cdot c_{HG} - 0.21 \cdot c_{HB} + 0.11 \cdot c_{HWB}$
6090	$-0.12 \cdot c_{HW} - 0.98 \cdot c_{Hq3} - 0.11 \cdot c_{Hu}$
124	$-0.20 \cdot c_{HWB} + 0.30 \cdot c_{Hq1} + 0.14 \cdot c_{Hq3} - 0.85 \cdot c_{Hu} + 0.29 \cdot c_{Hd}$
34	$-0.21 \cdot c_{Hbox} - 0.56 \cdot c_{HW} - 0.24 \cdot c_{HWB} - 0.11 \cdot c_{Hl1} + 0.51 \cdot c_{Hl3} - 0.16 \cdot c_{Hq1} + 0.17 \cdot c_{Hu} - 0.37 \cdot c_{ll1} - 0.10 \cdot \lvert c_{dH}\rvert + 0.25 \cdot \lvert c_{uG}\rvert - 0.12 \cdot c_{qq3}1$
22	$-0.11 \cdot c_G + 0.60 \cdot c_{HW} - 0.12 \cdot c_{HB} + 0.18 \cdot c_{Hl3} + 0.63 \cdot \lvert c_{uG}\rvert - 0.13 \cdot c_{qq11} - 0.31 \cdot c_{qq31} - 0.13 \cdot c_{uu1}$
16	$-0.48 \cdot c_{HW} + 0.19 \cdot c_{HB} + 0.11 \cdot c_{HWB} + 0.13 \cdot c_{Hl1} - 0.47 \cdot c_{Hl3} - 0.11 \cdot c_{He} + 0.31 \cdot c_{ll1} + 0.14 \cdot \lvert c_{dH}\rvert + 0.49 \cdot \lvert c_{uG}\rvert - 0.24 \cdot c_{qq31} - 0.10 \cdot c_{uu1}$
5	$0.13 \cdot c_{Hbox} - 0.14 \cdot c_{HDD} - 0.33 \cdot c_{HB} - 0.58 \cdot c_{HWB} - 0.42 \cdot c_{Hl1} - 0.34 \cdot c_{Hl3} + 0.33 \cdot c_{He} - 0.24 \cdot c_{Hq1} + 0.11 \cdot c_{ll1} - 0.17 \cdot \lvert c_{eH}\rvert$
0.9	$0.12 \cdot c_{HWB} + 0.26 \cdot c_{Hq1} - 0.21 \cdot c_{ll1} - 0.79 \cdot \lvert c_{eH}\rvert + 0.47 \cdot \lvert c_{dH}\rvert$
0.4	$0.18 \cdot c_{Hbox} - 0.11 \cdot c_{HW} + 0.12 \cdot c_{HWB} - 0.33 \cdot c_{Hl1} - 0.16 \cdot c_{Hl3} + 0.26 \cdot c_{He} + 0.67 \cdot c_{Hq1} + 0.18 \cdot c_{Hu} - 0.20 \cdot c_{Hd} - 0.12 \cdot c_{ll1} - 0.43 \cdot \lvert c_{dH}\rvert$
0.2	$-0.34 \cdot c_{Hbox} - 0.23 \cdot c_{Hl1} + 0.22 \cdot c_{Hl3} + 0.15 \cdot c_{He} + 0.32 \cdot c_{Hq1} + 0.11 \cdot c_{Hu} - 0.11 \cdot c_{Hd} + 0.40 \cdot c_{ll1} + 0.37 \cdot \lvert c_{eH}\rvert + 0.57 \cdot \lvert c_{dH}\rvert$

Table 8: Eigenvectors corresponding to the largest eigenvalues of the Fisher information matrix of the combined measurement of Ref. [5], expressed as a function of Wilson coefficients. The matrix is obtained by the propagation the Fisher information matrix of the STXS measurement to the Wilson coefficients. Both the production cross-sections and decay branching fractions are parametrised as a function of the Wilson coefficients. Only Wilson coefficients with a factor larger than 10% are listed for each eigenvector. The acceptance dependence on the Wilson coefficients is neglected in the parametrisation.

3.2.1 c_{HW}, c_{HB} and c_{HWB}

The three operators describing the interaction between the Higgs boson and the vector bosons: c_{HW}, c_{HB} and c_{HWB} are very strongly correlated. Even though c_{HW} is slightly constrained by VBF and VH, the sensitivity is driven mainly by Higgs boson decay processes, in particular in the $H \to \gamma\gamma$ channel. The analytic expression of the $H \to \gamma\gamma$ decay width in the CP-even case is given by [14]:

$$\frac{\Gamma(H \to \gamma\gamma)}{\Gamma_{\mathrm{SM}}(H \to \gamma\gamma)} \approx \left|1 + K_\gamma \mathscr{C}_{\gamma\gamma}\right|^2, \tag{12}$$

where K_γ is a constant describing the contribution of top-quark and W-boson loops to $H \to \gamma\gamma$, and

$$\mathscr{C}_{\gamma\gamma} = \frac{1}{\bar{g}_2^2} c_{HW} + \frac{1}{\bar{g}_1^2} c_{HB} - \frac{1}{\bar{g}_1 \bar{g}_2} c_{HWB}, \tag{13}$$

where $\bar{g}_{1,2}$ are the coupling constants for the SM $SU(2)_L$ and $U(1)_Y$ interactions included in the SMEFT Lagrangian.

The Wilson coefficient c_{HWB} can be related to the oblique electroweak correction parameter ΔS [15] as

$$\frac{v^2}{\Lambda^2} c_{HWB} = \frac{g_1 g_2}{16\pi} \Delta S. \tag{14}$$

ΔS is related to the weak mixing angle and is constrained by fits to electroweak data in Ref. [16] to $\Delta S \in [-0.06, 0.07]$. According to this result and for the sake of simplicity in the following c_{HWB} is fixed to zero. In future extension of this work its value will be profiled in the fit accounting for the constraint interval.

The remaining parameters c_{HW} and c_{HB} are fully anti-correlated in the fit and therefore cannot be measured independently. Figure 4 shows the two-dimensional scans in the plane of c_{HW} versus c_{HB} of the negative log-likelihood for the STXS measurements in the $H \to \gamma\gamma$ channel and for the combination of all decay channels, in the case of all decay branching ratios fixed to the SM. The figure shows that the correlation is fully dominated by the $H \to \gamma\gamma$ process.

According to Equation 13, the measurement should be sensitive to the combination $\frac{1}{\bar{g}_2^2} c_{HW} + \frac{1}{\bar{g}_1^2} c_{HB}$, which in the SM is approximately given by $0.27 c_{HW} + 0.96 c_{HB}$. This combination can be approximately identified, up to overall multiplicative factors, in the eigenvector combinations of Table 5, as well as in the leading eigenvectors from Tables 7 and 8. Figure 4 (d) shows a likelihood scan in the plane of this and the orthogonal combination. Both combinations are constrained in the fit, but with weaker sensitivity for the orthogonal combination.

3.2.2 c_{Hl1} and c_{He}

The parameters c_{Hl1} and c_{He} are almost exclusively constrained by the ZH production mode with a leptonic Z decay and the $H \to b\bar{b}$ Higgs boson decay process, as well as the $H \to 4\ell$ mode. In all regions sensitive to these processes, the effects of these two Wilson coefficient are almost equal in magnitude, and with opposite sign, as can be seen in the rows relative to $qq/gg \to H\ell\ell$ in Table 3 and to $H \to 4\ell$ in Table 5. The measurement is therefore mainly sensitive to their difference while their sum corresponds to a flat direction and is fixed to 0.

3.2.3 c_{Hq1}, c_{Hu} and c_{Hd}

The parameters c_{Hq1}, c_{Hu} and c_{Hd} are strongly correlated with each other. The eigenvectors are found from the covariance matrix calculated in a statistics-only fit where only these 3 parameters are allowed to vary. It has been checked that these correlations are not strongly affected by the systematic uncertainties. The obtained eigenvectors are:

$$\mathrm{EV}_1 = -0.3 c_{Hd} + 0.9 c_{Hu} - 0.3 c_{Hq1}, \tag{15}$$

$$\mathrm{EV}_2 = 0.3 c_{Hd} - 0.2 c_{Hu} - 0.9 c_{Hq1}, \tag{16}$$

$$\mathrm{EV}_3 = -0.9 c_{Hd} - 0.4 c_{Hu} - 0.2 c_{Hq1}. \tag{17}$$

The sensitivity to each of them can be estimated from the corresponding eigenvalues. Only EV_1 has sizable sensitivity in the final fit, while EV_2 and EV_3 are set to zero. The measured eigenvector is compatible with the expectations from the production mode parametrisation (see Table 3) and the sensitivity study (see Table 8). The constraint to these coefficients is coming mainly from VBF and ZH. In most of these STXS bins c_{Hq1} and c_{Hd} contribute to the eigenvector with the same sign, and with very similar A_i values. Conversely, c_{Hu} typically appears with an opposite sign with respect to c_{Hq1} and c_{Hd}, and with a larger A_i. This behavior is in particular reflected in the first of the eigenvalues obtained.

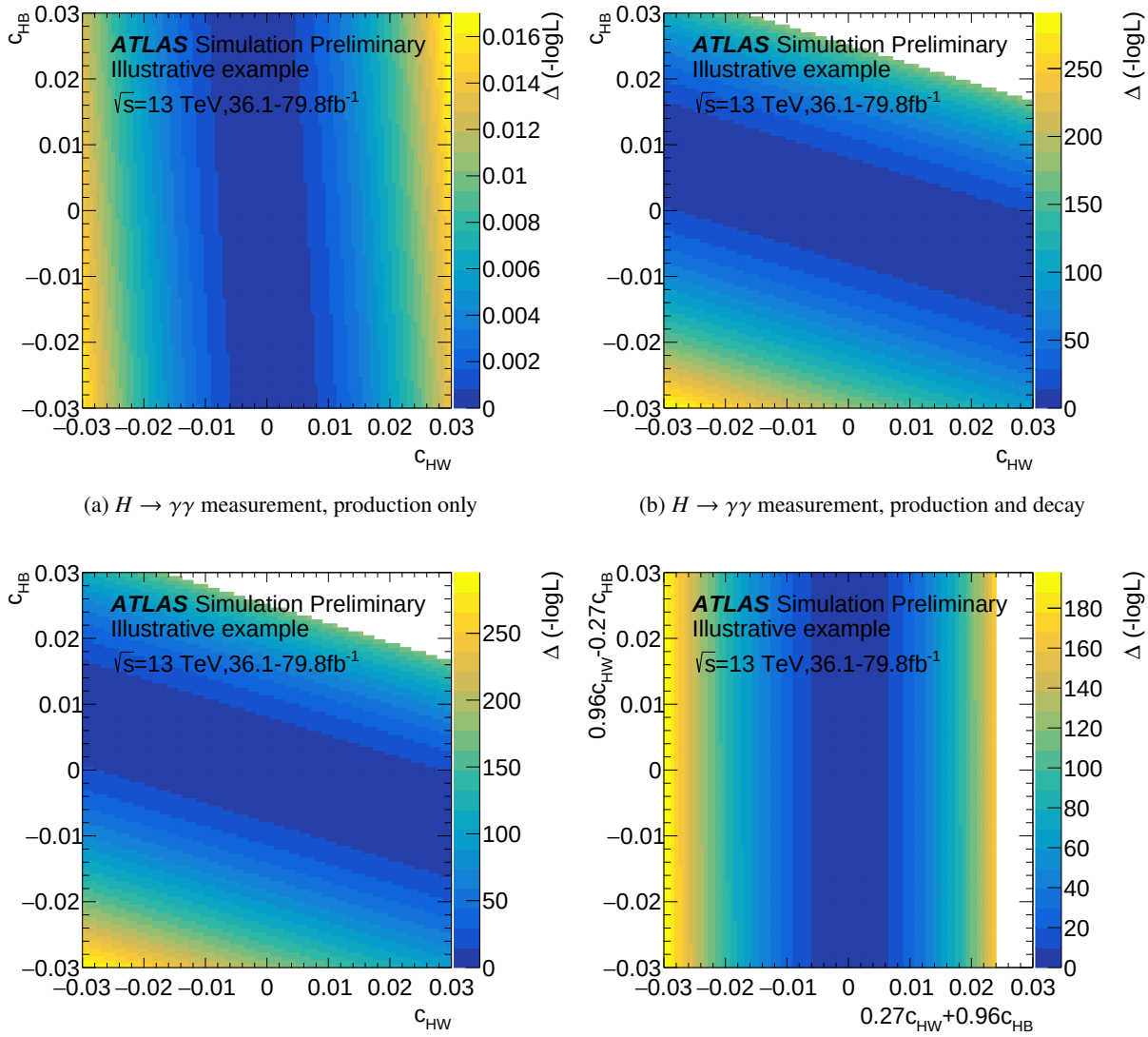

(a) $H \to \gamma\gamma$ measurement, production only

(b) $H \to \gamma\gamma$ measurement, production and decay

(c) Combined measurement, production and decay

(d) Combined measurement, production and decay, rotated

Figure 4: Panels (a), (b) and (c) show the two-dimensional scans in the plane of c_{HW} and c_{HB} of the negative log-likelihood for the $H \to \gamma\gamma$ STXS measurement ((a) and (b)) and the combined STXS measurement (c). In panel (a), only the production cross-sections are parametrised as a function of SMEFT Wilson coefficients, while in panel (b) the decay branching fractions are parametrised a well. The white area corresponds to the values of c_{HW} and c_{HB} leading to a negative signal yield. Panel (d) shows the two-dimensional scan of the negative log-likelihood of the combined STXS measurement in the plane of two orthogonal combinations of c_{HW} and c_{HB}. Both combinations are weakly correlated with other operators in the fit. The white areas correspond to the values of the sum leading to a negative signal yield.

3.2.4 Additional constraints

In the same way as for c_{HWB}, c_{HDD} can be related to the oblique parameter ΔT as follows [16]:

$$\frac{v^2}{\Lambda^2} c_{HDD} = -\frac{g_1 g_2}{2\pi(g_1 + g_2)} \Delta T, \tag{18}$$

and is thus fixed to 0.

The two operators O_{Hbox} and O_{ll1} are introduced in the parametrisation by the redefinition of the Higgs field and electroweak parameters in the SMEFT framework. They thus impact the overall normalization in the same way in most bins and are fully correlated. Due to further loop suppressions in ggF and $H \to \gamma\gamma$ decay vertices by $\frac{1}{16\pi^2 \cdot \Lambda^2}$, the impact on the amplitudes from O_{ll1} and O_{Hbox} are suppressed compared to LO processes and are neglected in the SMEFTsim tool:

- c_{ll1} mainly enters the parametrisation in corrections of electroweak parameters, like G_F, which is an input parameter. No sensitivity to this operator is expected from Higgs boson measurements, and it can be constrained much better in electroweak measurements. c_{ll1} is thus set to zero in the fit.
- c_{Hbox} is introduced in the redefinition of the Higgs field. It therefore appears with the same coefficient in all production modes and decay channels, except $gg \to H$ and $H \to \gamma\gamma$, where its contribution is zero. This parameter therefore introduces mainly an overall normalization difference and can not be measured together with the other parameters.

3.2.5 Measurement parameters for the combined measurement with production and decay parametrisation

In light of the sensitivity studies listed in the previous sections, the following combinations of SMEFT Wilson coefficients should be considered for the interpretation of the combined STXS measurement:

- c_{HG}
- c_{Hq3}
- $0.27 c_{HW} + 0.96 c_{HB}$
- $0.96 c_{HW} - 0.27 c_{HB}$
- $|c_{uG}|$
- c_{Hl3}
- $c_{Hl1} - c_{He}$
- $|c_{eH}|$
- $|c_{dH}|$
- $-0.3 c_{Hd} + 0.9 c_{Hu} - 0.3 c_{Hq1}$

This list has nevertheless to be considered as an illustrative example, since the methodology presented in this note only represents a snapshot of an ongoing effort that will be improved in the future.

4 Conclusions

A technique to interpret simplified template cross-sections measurements within the context of the SMEFT is presented. Parametrisations of the impact on the Higgs sector of BSM phenomena introduced within the SMEFT framework are developed, both for the Higgs boson production cross sections and decay widths. Techniques have been presented to determine the combinations of SMEFT parameters to which the measurements are sensitive. These also allow to identify flat directions in the fit, along which the measurements provide no sensitivity. This information should allow to perform reinterpretations of the ATLAS STXS measurements in a way that does not suffer from numerical issues associated with flat directions, and does not rely on SMEFT model assumptions.

The presented methodology relies on a series of assumptions (e.g. no dependence on the acceptance selections of the SMEFT parameters, strong external constraints on some parameter) that need further investigation, and call for improvements to the technique. For this reason, all presented results should be considered as illustrative examples, mainly meant to steer discussion within the community.

References

[1] J. R. Andersen et al., *Les Houches 2015: Physics at TeV Colliders Standard Model Working Group Report*, (2016), arXiv: 1605.04692 [hep-ph] (cit. on p. 2).

[2] LHC Higgs Cross Section Working Group, D. de Florian et al., *Handbook of LHC Higgs Cross Sections: 4. Deciphering the Nature of the Higgs Sector*, (2016), arXiv: 1610.07922 [hep-ph] (cit. on p. 2).

[3] I. Brivio, Y. Jiang and M. Trott, *The SMEFTsim package, theory and tools*, JHEP **12** (2017) 070, arXiv: 1709.06492 [hep-ph] (cit. on pp. 2, 3).

[4] B. Grzadkowski, M. Iskrzynski, M. Misiak and J. Rosiek, *Dimension-Six Terms in the Standard Model Lagrangian*, JHEP **10** (2010) 085, arXiv: 1008.4884 [hep-ph] (cit. on p. 2).

[5] The ATLAS Collaboration, *Combined measurements of Higgs boson production and decay using up to 80 fb^{-1} of proton-proton collision data at $\sqrt{s}$ = 13 TeV collected with the ATLAS experiment*, (2019), arXiv: 1909.02845 [hep-ex] (cit. on pp. 2–4, 8, 11, 14, 15).

[6] C. Hays, V. Sanz Gonzalez and G. Zemaityte, *Constraining EFT parameters using simplified template cross sections*, tech. rep. LHCHXSWG-2019-004, CERN, 2019, URL: https://cds.cern.ch/record/2673969 (cit. on p. 2).

[7] A. Alloul, B. Fuks and V. Sanz, *Phenomenology of the Higgs Effective Lagrangian via FEYNRULES*, JHEP **04** (2014) 110, arXiv: 1310.5150 [hep-ph] (cit. on p. 2).

[8] ATLAS Collaboration, *Measurements of Higgs boson properties in the diphoton decay channel with 80 fb^{-1} of pp collision data at $\sqrt{s}$ = 13 TeV with the ATLAS detector*, (2018), ATLAS-CONF-2018-028, URL: http://cdsweb.cern.ch/record/2628771 (cit. on pp. 2, 4, 11, 13, 14).

[9] J. Alwall et al., *The automated computation of tree-level and next-to-leading order differential cross sections, and their matching to parton shower simulations*, JHEP **07** (2014) 079, arXiv: 1405.0301 [hep-ph] (cit. on p. 3).

[10] C. Degrande, B. Fuks, K. Mawatari, K. Mimasu and V. Sanz, *Electroweak Higgs boson production in the standard model effective field theory beyond leading order in QCD*, Eur. Phys. J. **C77** (2017) 262, arXiv: 1609.04833 [hep-ph] (cit. on p. 3).

[11] T. Sjöstrand, S. Mrenna and P. Z. Skands, *A brief introduction to PYTHIA 8.1*, Comput. Phys. Commun. **178** (2008) 852, arXiv: 0710.3820 [hep-ph] (cit. on p. 3).

[12] F. James and M. Winkler, *MINUIT User's Guide*, (2004), URL: https://inspirehep.net/record/1258345/files/mnusersguide.pdf (cit. on p. 11).

[13] G. Cowan, K. Cranmer, E. Gross and O. Vitells, *Asymptotic formulae for likelihood-based tests of new physics*, Eur. Phys. J. C **71** (2011) 1554, arXiv: 1007.1727 [physics.data-an], Erratum: Eur. Phys. J. C **73** (2013) 2501 (cit. on p. 12).

[14] I. Brivio and M. Trott, *The Standard Model as an Effective Field Theory*, Phys. Rept. **793** (2019) 1, arXiv: 1706.08945 [hep-ph] (cit. on p. 15).

[15] M. E. Peskin and T. Takeuchi, *Estimation of oblique electroweak corrections*, Phys. Rev. D **46** (1 1992) 381, URL: https://link.aps.org/doi/10.1103/PhysRevD.46.381 (cit. on p. 15).

[16] J. Ellis, C. W. Murphy, V. Sanz and T. You, *Updated Global SMEFT Fit to Higgs, Diboson and Electroweak Data*, JHEP **06** (2018) 146, arXiv: 1803.03252 [hep-ph] (cit. on pp. 16, 18).